Materials Today Communications 36 (2023) 106645

Contents lists available at ScienceDirect

Materials Today Communications

journal homepage: www.elsevier.com/locate/mtcomm

Sustainable manufacturing of new construction material from alkali activation of volcanic tuff

Cengiz Bagci [a], Giulia Tameni [b], Hamada Elsayed [b], Enrico Bernardo [b,*]

[a] Hitit University, Corum, Turkey
[b] Department of Industrial Engineering, University of Padova, Padova, Italy

ARTICLE INFO

Keywords:
Tuff
Alkali activation
Gelation
Sintering

ABSTRACT

The current climate emergency leads to reduction of virgin raw material extraction and promotes circular economy. In this framework, alkali activation of unemployed fraction of grey tuff, combined with glass waste, provides a range of sustainable construction materials. For the sake of sustainability, tuff powder was subjected to rapid attack (30 min), operated by a 'weak' alkaline solution (3 M NaOH), and then left to dry at low temperature (75 °C) for 72 h. The addition of Triton X-100 surfactant was considered to obtain foams starting from slurries with different liquid-to-solid ratio. A thermal treatment was applied to selected samples, at low temperature (700 °C). Despite the 'mild' activation conditions, all products survived after immersion in boiling water or acid solution, already in the unfired state, according to the formation of a multiphasic gel. The strength-to-density ratio, especially for foams, in both unfired and fired form, compares well with that of already existing construction materials (e.g. it could exceed 5 MPa cm^3/g).

1. Introduction

One of the most beneficial approaches to solid waste reduction is industrial ecology [1]. Ordinarily industrial waste or unemployed materials cannot be directly used, but in a circular economy prospective they may be combined in an up-cycling perspective. Up-cycling is a process that converts low-value substances into higher-value products, with limited energy and materials inputs. The building sector is one of the most environmentally impacting industrial fields: as an example, Portland cement production reckons for almost 5–7 % of the global carbon dioxide (CO_2) emission, as manufacturing one ton of cement (OPC) liberates one ton of carbon dioxide [2]. It is evident that the development of alternative binders is a fundamental ecological challenge.

A classical solution to reduce emissions and save both energy and natural mineral resources is the incorporation of supplementary cementing materials ('pozzolanic' materials, reacting with portlandite by-product from cement hydration), of natural and industrial origin [3]. A fundamental alternative is provided by binders featuring a completely different molecular structure, such as geopolymers. Geopolymers are produced according to the reaction between alumino-silicate feedstock, such as metakaolin, and concentrated solutions of alkali hydroxides or silicates. Alumino-silicate raw materials are firstly subjected to dissolution, due to the dismantling of Si-O and Al-O bonds; secondly, condensation reactions involving the dissolution products promotes the formation of a 'zeolite-like' gel, consisting of a continuous, three-dimensional alumino-silicate network, amorphous or crystalline, from the polymerization of SiO_4 and AlO_4 units (the latter being stabilized by alkali ions), sharing bridging oxygens [4].

The sustainability of the geopolymer approach increases when considering, instead of metakaolin, resulting from calcination of pure kaolin clay, heterogeneous systems of natural origin, such as laterite rock and clays [5,6] or volcanic ash [7–9], or industrial by-products, such as slags and fly ash from coal combustion [10], often used also as pozzolans. The above-mentioned network, as an effect of the remarkable iron oxide content in the feedstock, may comprise even FeO_4 units [7]. Alkaline attack may be even replaced by acid attack, e.g. by means of concentrated solutions of phosphoric acid, yielding PO_4 units [5,11].

Among volcanic materials, tuff is known for its multiple variants, resulting in different changing physical and mechanical properties [12]. Turkey has about 15.8 % of the global volcanic tuff reserves, with major amounts located in Anatolia peninsula (Eastern Anatolia and Central Anatolia), where intense volcanic activities took place [13,14]. Due to its high porosity, the local grey tuff variant can be used, in buildings, in

* Corresponding author.
E-mail address: enrico.bernardo@unipd.it (E. Bernardo).

https://doi.org/10.1016/j.mtcomm.2023.106645
Received 16 April 2023; Received in revised form 22 June 2023; Accepted 10 July 2023
Available online 12 July 2023
2352-4928/© 2023 The Author(s). Published by Elsevier Ltd. This is an open access article under the CC BY-NC-ND license (http://creativecommons.org/licenses/by-nc-nd/4.0/).

form of thermally insulating blocks [15]. The cutting of regular pieces from natural coarse blocks obviously generates powders, which can be considered a form of natural waste. A sustainable exploitation of this tuff occurs only in the perspective of application of the fine fraction, supported by the significant amounts of alumina and silica [16,17]. Nowadays, powders are used as masonry mortars and lightweight concretes, according to direct geopolymerization or formation of 'hybrid' binders (combined with ordinary Portand cement) [18,19]. The products are undoubtedly interesting, but it must be underlined that activation is generally performed by means of highly concentrated alkaline solutions, and with the support of additives. These components are necessary also for 'green' concrete (from 10 % to 15 %), resulting from the use of tuff simply as pozzolanic material [20].

In the perspective of sustainable manufacturing, also additives should consist of discarded materials. In this framework, glasses are interesting, since industrial practice contradicts the general perception of fully recyclable materials, by remelting. Due to issues in color sorting and the presence of impurities, remarkable amounts of waste glass are still disposed in landfills [21]. More precisely, heterogeneous contaminants (metallic, ceramic, polymeric particles) are mostly concentrated in the fine fraction of soda-lime cullet, resulting from purification of crushed containers [22]. The use as pozzolanic material, in concrete [21], or as component, in geopolymer-yielding mixtures [23] is interesting, but not exhaustive.

A possible weakness of alkali-activated materials, in terms of sustainability, concerns the molarity of activators, also comprising synthetic compounds, such as alkali silicates. As mentioned before, a common trend involves the extensive dissolution of the starting feedstock, operated by very concentrated activating solutions. As an example, natural volcanic pozzolan undergoes optimized activation after attack by a solution with a NaOH molarity equal to 8 mol/L (8 M) and Na_2SiO_3/NaOH ratio of 1.2 [24]; palm oil clinker is activated in even harsher conditions (14 M NaOH) [25]. This investigation aims at exploring the potential of 'weak' alkali activation, applied on grey tuff alone or combined with soda-lime glass waste. According to recent studies [22], mixtures of volcanic material and glass undergo gelation after activation with NaOH aqueous solution even at low molarity (3 M): unlike in many geopolymerization studies, the chemical attack is not intended to determine a substantial dissolution of the starting feedstock; on the contrary, the attack involves the activation of surfaces. Adjacent particles, according to condensation of surface gels, form strong chemical bonds (Si-O-Si, Si-O-Al, Al-O-Al), preventing any disintegration upon the immersion of samples in boiling water. We will show that grey tuff may be activated in weak alkali solution, with the definition of stable 'cold consolidated' blocks, with or even without the support of soda-lime glass. The process can be tuned, operating on solid/liquid ratio and the application of intensive mechanical stirring, for the definition of highly porous foams [26,27].

A thermal treatment at 700 °C is presented as further tuning possibility, to be used 'ab initio' or as a way to recycle end-of-life dense and porous 'unfired' products [22]. The adopted temperature was chosen as the minimum temperature for experiencing viscous flow sintering of soda-lime glass [26], far lower than one used for cheapest ceramics, such as clay bricks [28,29]. Selected samples were finally found to compare favorably with commercial building materials.

2. Materials and methods

Grey tuff (T) from Anatolia (Turkey) and soda-lime glass waste (SLG, provided by SASIL SpA, Biella, Italy) were selected as starting materials in form of fine particles (diameter < 75 μm). The chemical composition of raw materials, obtained using XRF analysis, is reported in Table 1. An alkaline solution, at a concentration of 3 mol/L (3 M), was prepared using commercial sodium hydroxide (Honeywell, North Carolina, USA).

To obtain consolidated samples, a solid phase consisting of tuff in 100 wt% or tuff and soda-lime glass in 50–50 wt%, was cast in alkaline solution to form slurries with liquid-to-solid ratio of 0.42. The slurries were stirred for 30 min at 450 rpm, and then cast in polymer moulds and cured for 72 h at 75 °C.

Foamed samples were prepared starting from slurries with different solid-to-liquid ratio (0.82–0.67–0.54), stirred at 900 rpm for 3 h, in plastic containers. The suspensions were left at 75 °C for 15 min (pre-foaming phase) and then added with 4 wt% of Triton X-100 surfactant (polyoxymethylene octyl phenyl ether, $C_{14}H_{22}O(C_2H_4O)_n$, n = 9–10, Sigma-Aldrich, Gillingham, UK) and subjected to intensive mechanical stirring (2000 rpm). The trapping of air bubbles, favored by surfactant, determined a substantial foaming [26,27]. Samples were dried at 40 °C for 48 h.

Selected samples were fired at 700 °C, for 1 h, with a heating rate of 2 °C/min. Expressly for foams, a intermediate step at 300 °C for 2 h, with a heating rate of 1 °C/min, was applied in order to degrade the surfactant.

Fourier-transform infrared spectroscopy and X-ray diffraction were performed to evaluate the phases developed during alkali activation and subsequent foaming process. FTIR spectra were collected using Jasco 4200 FTIR spectrometer (Jasco, Japan) and measurement were acquired in the 4500–400 cm^{-1} region. XRD (Bruker D8 Advance, Karlsruhe, Germany - CuKα radiation, 0.15418 nm, 40 kV-40 mA, $2\theta = 9–70°$, step size 0.02°, 2 s counting time) was used for mineralogical analysis. Match! ® program package (Crystal Impact GbR, Bonn, Germany), operating with the PDF-2 database (ICDD-International Centre for Diffraction Data, Newtown Square, PA, USA) supported the phase identification.

Compressive tests were performed on specimens (10 mm × 10 mm × 10 mm, at least 5 for each batch), cut from larger samples, using universal material testing machine (Quasar 25, Galdabini, Cardano, Italy) with a crosshead speed of 1 mm/min. The geometrical density (ρ_{geom}) was calculated as ratio between the mass and the volume of samples; the apparent density (ρ_{app}) and the true density (ρ_{true}) were measured using helium pycnometer (Micromeritics AccuPyc 1330, Norcross, GA, USA) operating on bulk or crushed samples, respectively. These density data were used to calculate the value of open and close porosity. CES (Cambridge Engineering Selector) software package (Granta EduPack, Ansys Granta, Canonsburg, PA, USA) was used to obtain the strength-to-density trade-off chart adopted to compare new alkali activated materials (unfired and fired) with existing commercially available construction materials.

The morphology and the microstructure of samples were assessed by optical stereomicroscopy (AxioCam ERc 5 s Microscope Camera, Carl Zeiss Microscopy, Thornwood, New York, USA) and scanning electron microscopy (FEI Quanta 200 ESEM, Eindhoven, The Netherlands).

To evaluate gel stability, both boiling test and acid attack were performed. Cubic samples were immersed in distilled water, at 100 °C, or in a solution of HCl (pH=5), to establish integrity in harsh conditions.

Table 1
Chemical composition of grey tuff and soda-lime glass.

Oxides [%]	SiO_2	Al_2O_3	Fe_2O_3	TiO_2	CaO	MgO	Na_2O	K_2O	P_2O_5	Mn_2O_3	SO_3
Tuff	43.5	14.1	12.3	2.3	8.3	10.4	2.0	1.5	0.45	0.11	0.06
SLG	72	3.2	0.42	0.07	10	2.3	12	1	–	–	–

3. Results and discussion

3.1. Cold consolidated samples

As received tuff did not feature a uniform particle distribution. Relatively coarse particles (with a diameter of 10–15 μm) were accompanied by a multitude of smaller particles (Fig. 1a). The alkali activation (Fig. 1b) did not determine any significant dissolution, even of finer particles; it basically caused the development of a thin layer of surface gel, binding particles to each other. This is evident especially from the surface of coarser particles: in the as received state particles exhibit smooth, vitreous surfaces (Fig. 1a); on the contrary, the surface of coarser particles, after activation, exhibited some texturing (Fig. 1b).

The transformations occurring upon activation were first monitored by means of X-ray diffraction analysis, shown in Fig. 2a. As received tuff, in analogy with other volcanic materials (such as volcanic ash from Mt. Etna [22]), featured main lines attributable to plagioclase feldspar ($Ca_{0.72}Na_{0.28}Al_{1.72}Si_{2.28}O_8$, PDF#89-1468). Plagioclase is a solid solution between sodium feldspar (albite, $NaAlSi_3O_8$) and calcium feldspar (anorthite, $CaAl_2Si_2O_8$), with a Na/Ca ratio of approximately 1:4. Other peaks are consistent with a pyroxene solid solution (diopside ferrian, $Ca_{1.022}Mg_{0.857}Fe_{0.266}Si_{1.877}O_6$, PDF#89-0834), quartz ($SiO_2$, PDF#85-1780) and calcium aluminum silicate hydrate (stellerite B, $Ca_{6.4}Mg_{15.9}O_{146.56}H_{8.24}$, PDF#71-1874). The latter phase, belonging to the vast class of zeolites, is accompanied by traces of other zeolites, based on sodium (natrolite, $Na_2Al_2Si_3O_{12}H_2$, PDF#80–1572, and unnamed zeolite, $Na_{0.5}H_{0.5}AlSi_2O_6$, PDF#80-1394).

Alkali activation did not determine significant transformations in the mineralogical structure (Fig. 2a); the most relevant changes are associated with the height of feldspar main peak ($2\theta \sim 28°$). This could be due to the partial dissolution of feldspar upon alkaline attack, known to be insensitive to the Ca-Na proportion [30]. The condensation of reaction products, during drying step, evidently promoted the rebuilding of strong Si-O-Si and Si-O-Al bonds: hardened samples did not degrade substantially, after immersion in boiling water or in HCl (pH=5). The crystal phases, already detected after activation, were confirmed, with the notable increase of the signal-to-noise. In our opinion, this was due to the formation of a mixed gel: the increase in the signal could come from a reduced amount of amorphous phase. SiO_4 and AlO_4 units, originally present in feldspar and put in solution after alkaline attack, reorganized in the gel surrounding unreacted particles (see Fig. 3a). While a highly polymerized fraction (SiO_4 bound with AlO_4, the latter stabilized by Na^+ ions) survived to boiling water and acid, a depolymerized fraction (concentrating alkali ions) was removed (see the slightly more abundant voids, in the gel between unreacted particles, in Fig. 3b,c).

Soda-lime glass (practically Al_2O_3-free, in 1:1 proportion with tuff) was first conceived to drastically reduce the nominal Al_2O_3/SiO_2 content and thus the capability to stabilize alkali ions, coordinated with AlO_4 units. Despite this, drying of alkali activated tuff/glass suspensions still yielded a stable material, resisting to boiling water. For this sample, the intensity of quartz and pyroxene peaks remained practically unaltered (Fig. 2b), despite the sensible reduction of tuff; the addition of soda-lime glass evidently promoted an increase of amorphous fraction.

FTIR spectroscopy provided additional information regarding the consolidation mechanism. As illustrated by Fig. 4a, as received, activated and 'boiled' tuff samples share the most intense band centred at approximately 1000 cm^{-1}, corresponding to Si-O-Si or Si-O-Al asymmetric vibration. A secondary band, located at 880 cm^{-1}, is attributed to overlapping of Al-OH and Si-OH vibration signals [31–,32,33]. The alkali activation actually determined some broadening and (slight) downshifting of the main band, consistent with the formation of a gel with mixed ions [34]. The presence of the band at 1400 cm^{-1} is attributed to C-O bond stretching, typical of inorganic carbonates, evidently present as amorphous material [35]. The observed reduction of the C-O related band, with boiling, is consistent with the solubility of (hydrated) carbonates. As shown in Fig. 4b, the 'dilution' of tuff with soda-lime glass, entailed shifts in both main and carbonate bands, likely due altered balances between Al^{3+} and Si^{4+} ions and between Ca^{2+} and Na^+ ions.

As reported in Table 2, the porosity of samples from activated tuff and tuff/glass mixture, mostly open, approached 40 vol%. The geometrical density is in the range of that exhibited by structural lightweight concrete; the correlation with compressive strength (in the order of 2 MPa) should be evaluated in the perspective of possible application in constructions. The graph in Fig. 5 displays the delicate trade-off between density and compressive strength of commercial construction materials: materials with the highest porosity content typically exhibit the lowest strength values (and highest values of 1/compressive strength) and viceversa. A solution can be considered as 'non-dominated' [36] when, at a given value of density, it provides the highest strength; as an alternative, a 'non-dominated' solution, at a given strength, offers the lowest density. Hardened tuff and tuff/glass mixture were actually far from offering an optimized situation; with the same density, as an example, they were much weaker than structural lightweight concrete. It should be noted, however, that the newly developed materials were 'binder-only' systems, i.e. they did not contain any aggregate (sand or crushed stone); in the same strength range, they were only slightly denser than insulating lightweight concrete.

A firing treatment was applied to study any possibility of further consolidation, by viscous flow sintering. For the sake of sustainability, the treatment was performed at only 700 °C, i.e. far below the

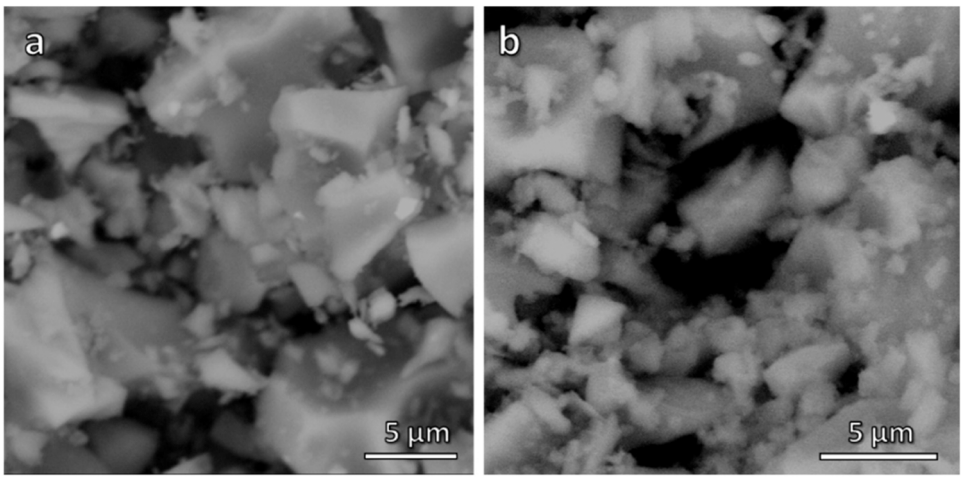

Fig. 1. Grey tuff before alkali activation (a) and after activation and drying (b).

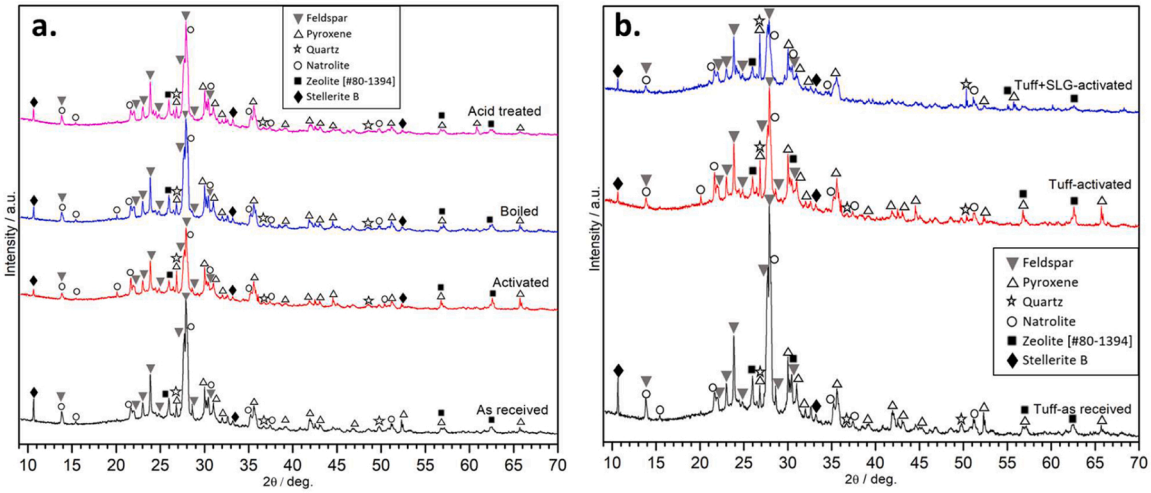

Fig. 2. Phase evolution from alkali activation of tuff: a) stability after boiling water test and acid attack; b) effect of SLG addition.

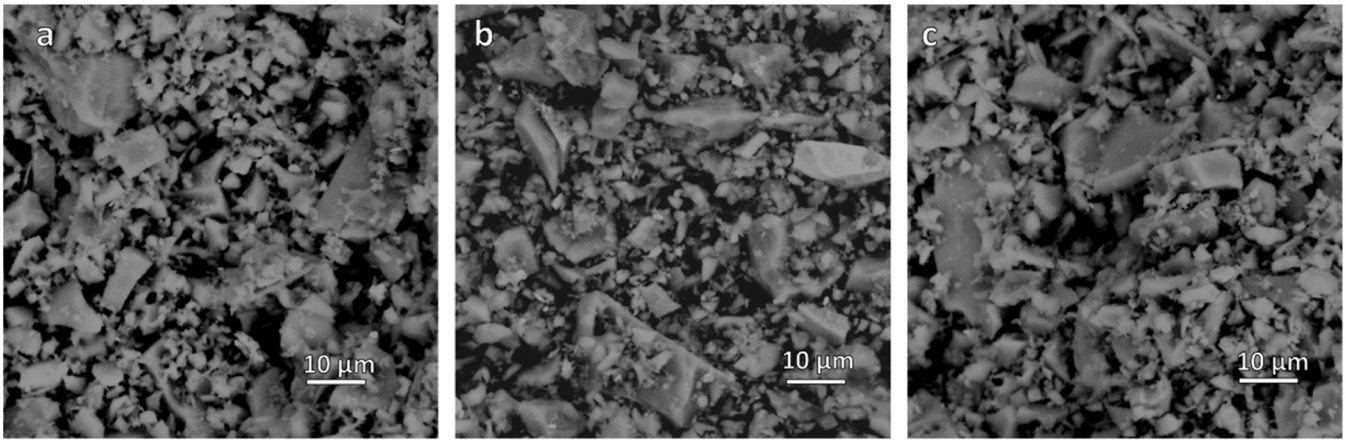

Fig. 3. Microstructural details of tuff (a) activated (b) boiled (c) acid treated.

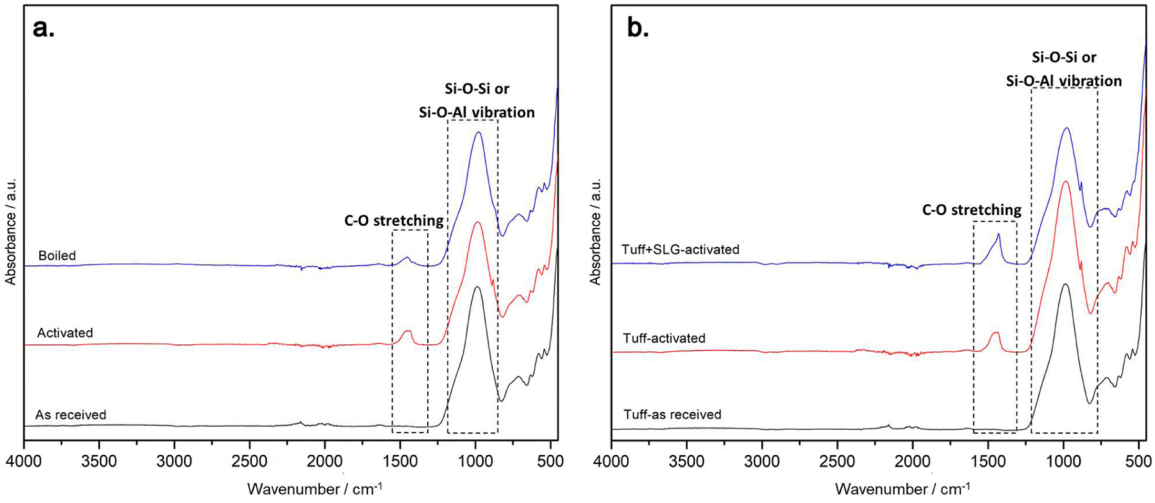

Fig. 4. FTIR diffraction patterns obtained for (a) tuff in different analyzed conditions (b) tuff and tuff+SLG after alkali activation.

temperatures (>850 °C [28]) adopted for the sintering of clay bricks, and corresponding to the minimum temperature for the pressure-less sintering of soda-lime glass [27].

As received tuff did not exhibit any densification (Fig. 6a). On the contrary, the activated material exhibited some binding of adjacent particles (Fig. 6b): the thin layer of gel, binding particles already after activation, evidently transformed into liquid phase, favouring sintering despite the low temperature. As shown by Table 2 and Fig. 5, fired tuff

Table 2
Physical and mechanical properties of 'dense' samples.

Sample type	Density [g/cm^3]	Total porosity (vol%)	Open porosity (vol%)	Closed porosity (vol%)	Compressive strength [MPa]
Tuff	1.58 ± 0.09	39.8 ± 0.1	39.3 ± 0.1	0.5 ± 0.1	1.8 ± 0.3
Tuff+SLG	1.56 ± 0.07	39.8 ± 0.1	38.9 ± 0.1	0.9 ± 0.1	2.4 ± 0.9
Tuff_fired	1.76 ± 0.1	34.1 ± 0.1	28.6 ± 0.1	5.5 ± 0.1	2.0 ± 0.2
Tuff+SLG_fired	1.16 ± 0.1	53.5 ± 0.1	30.6 ± 0.1	22.9 ± 0.1	2.3 ± 0.4

(after activation) exhibited a slight densification and a slight increase of compressive strength, compared to activated material; the liquid phase allowed just for some 'necking' of adjacent particles, leaving an abundant open porosity. Enhanced viscous flow sintering was observed with the glass-modified mixture (Fig. 6c); the softening of soda-lime glass provided, already at 700 °C, an abundant liquid phase. This phase promoted the formation of uniform pyroplastic mass, which could more effectively trap gasses released by dehydration reactions occurring to the compounds developed upon activation. As shown by Fig. 5, activated and fired tuff/glass mixture overlaps with insulating lightweight concrete; we can think at granules of fired tuff/glass mixture as a possible filler in this type of concrete.

The firing at 700 °C was studied also in terms of mineralogical transformations (Fig. 7). Diffraction peaks ascribed to zeolites are not traceable, since these phases are known to decompose (by dehydration) above 500–550 °C [37]. In agreement with the thermal transformation of many alkali activated materials, dehydration likely promoted the crystallization of an anhydrous sodium aluminum silicate phase [nepheline (Si-rich), $Na_{6.8}(Al_{6.3}Si_{9.7}O_{32})$, PDF #79-0994]. Moreover, the ionic interdiffusion determined some evolution of the original feldspar phase: after firing the diffraction lines are consistent with the simultaneous presence of calcium aluminum silicate [anorthite, $Ca(Al_2Si_2O_8)$, #89-1462], with alkali left in potassium sodium calcium alumino-silicate [sanidine, $K_{0.42}N_{0.58}Ca_{0.03}(AlSi_3O_8)$, #89-1455]. This phase assemblage is confirmed also for the tuff/glass mixture.

3.2. Foamed samples

To obtain foamed samples, tuff was suspended in alkaline solution with increasing liquid-to-solid ratio. Changes in the latter had dramatic effects on the pore distribution, as shown by Fig. 8a,b: higher contents of solid obviously enhanced the viscosity, in turn limiting the coalescence of small air bubbles, embedded upon intensive mechanical stirring, into larger ones. No practical change was observed on the phase assemblage (Fig. 9a). The thermal transformation maintained the open-celled structure (Fig. 8c). As in cold consolidated dense samples, the diffraction analysis is consistent with the concurrent presence of anorthite and sanidine, accompanied by nepheline (Fig. 9b).

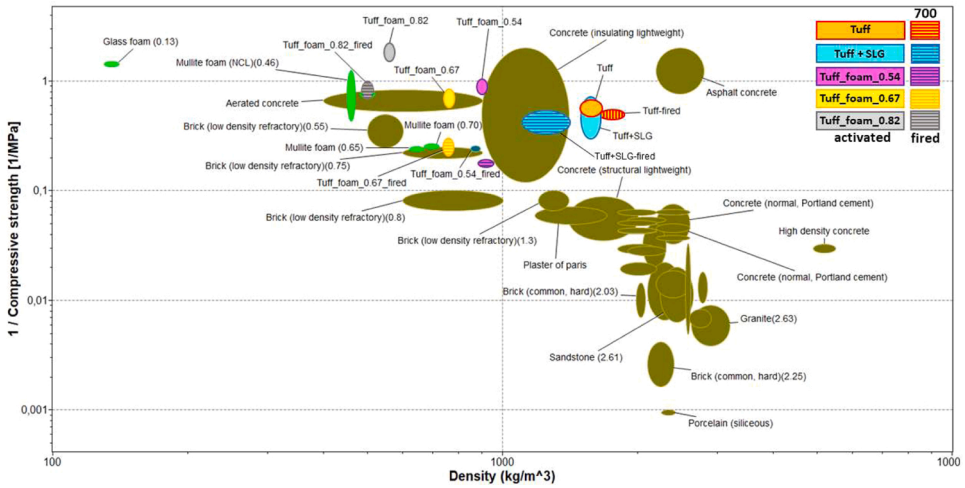

Fig. 5. Compressive strength/density trade-off of fired and unfired products (computed by means of CES software package).

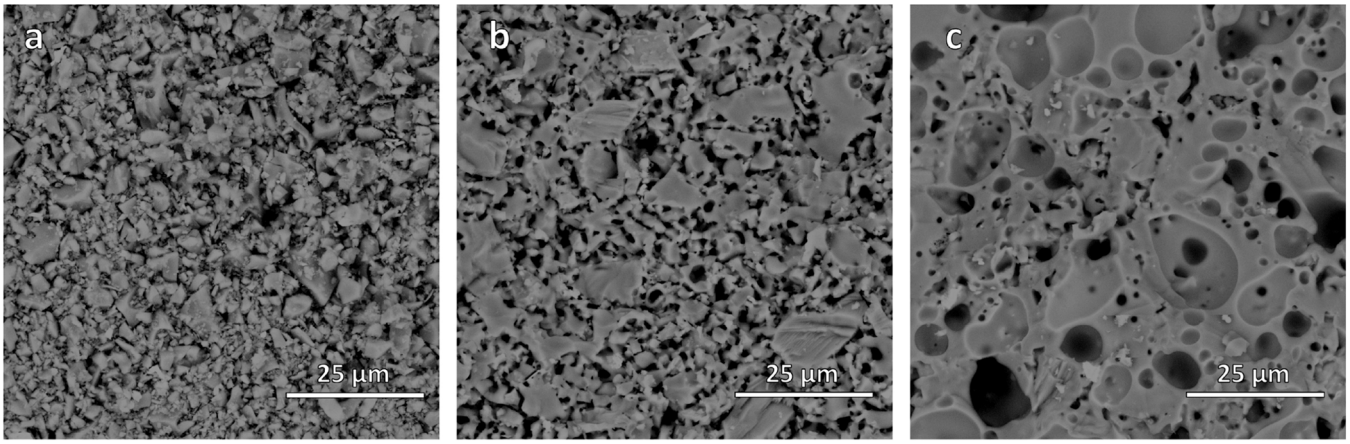

Fig. 6. Microstructural images of (a) Tuff fired before alkali activation (b) Tuff fired after alkali activation (c)Tuff+SLG fired after alkali activation.

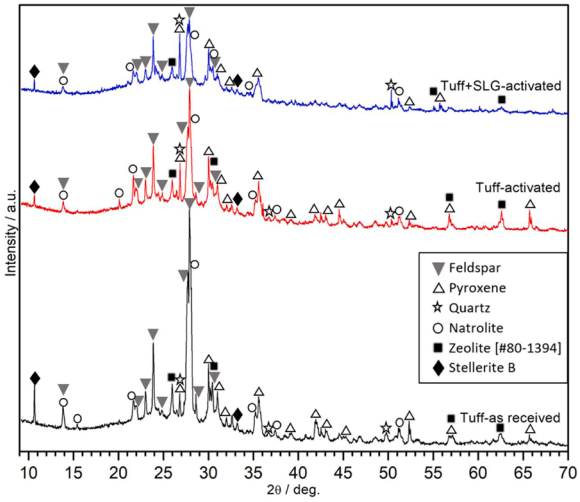

Fig. 7. X-ray diffraction patterns for fired samples of Tuff fired before alkali activation, after alkali activation and tuff+SLG fired after alkali activation.

Compared to dense samples, some differences emerged from FTIR spectroscopy (Fig. 10a). In all spectra, the main absorption band remained between 900 and 1100 cm^{-1}, attributed to the Si-O-Al and Si-O-Si asymmetric stretching vibrations [38]. The band at about 1450 cm^{-1}, associated with C-O bond is much more pronounced, is referred to the carbonate formed by the reaction between alkali and CO_2 [39]. Finally, a wide band in the 3000–3500 cm^{-1} interval is due O-H stretching vibrations, probably due to atmospheric humidity or hydrated species. The peak absorbance at 2900 cm^{-1} represents the C-H stretching vibration from the surfactant used in foaming process [27]. Vibrations attributable O-H, C-H and C-O bonds were absent after firing (Fig. 10b). The more abundant formation of hydrated sodium carbonate (not detected by XRD analysis), in form of needles, is confirmed by high magnification electron microscopy (Fig. 11a); again, firing did not determine, in the absence of glass, a substantial viscous flow, resulting in foams with porous struts (Fig. 11b).

As reported in Table 3, the porosity remained, in all conditions, predominantly open. This allowed an interesting calculation, starting from the experimental values of compressive strength. According to the Gibson-Ashby model [40], an open-celled body can be approximated by a lattice of interconnected dense beams. The compressive strength σ_c depends on the bending strength σ_{bend} of the solid forming the same beams ('bending strength of the solid phase'), combined with the relative density (ratio between geometrical and true densities ρ_{rel} = (100-TP)/100; TP is the total porosity):

$$\sigma_c \approx \sigma_{bend} \cdot 0.2 \cdot (\rho_{rel})^{1.5}$$

Using the experimental data of relative density, the compressive strength could be fitted by 'apparent' values of σ_{bend}. It is interesting to note that for unfired foams σ_{bend} approached 50 MPa, which is substantial, considering that the bending strength of dense soda-lime glass is approximately 70 MPa [41]. Firing led to a notable improvement, with 'apparent' values of σ_{bend} even exceeding 100 MPa. The excellence of foamed products, especially after firing, is further testified by Fig. 5:

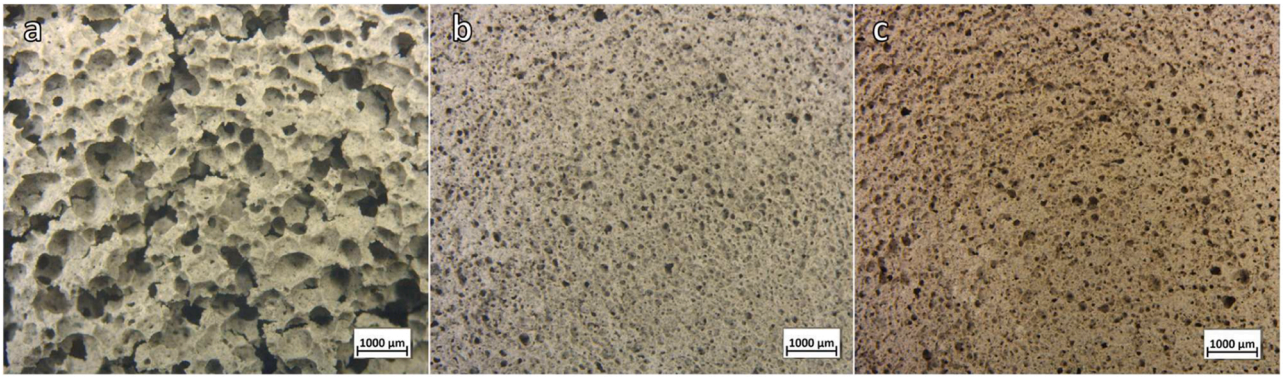

Fig. 8. Optical microscope images of (a) foam with w/s = 0.82 (b) foam with w/s = 0.54 (c) foam fired with w/s = 0.54.

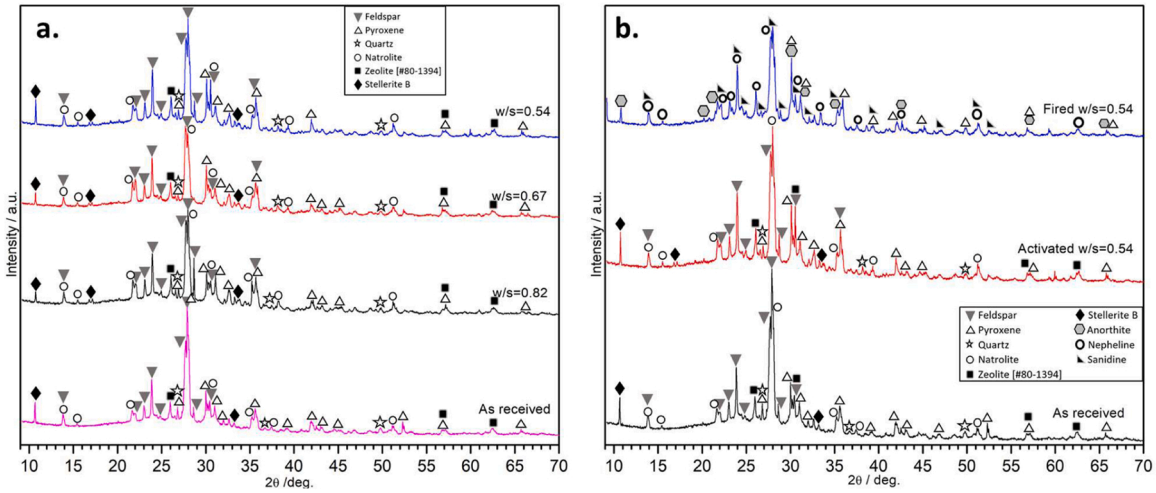

Fig. 9. X-ray diffraction patterns of foams: a) obtained starting from different liquid-to-solid ratio; b) transformed by firing at 700 °C.

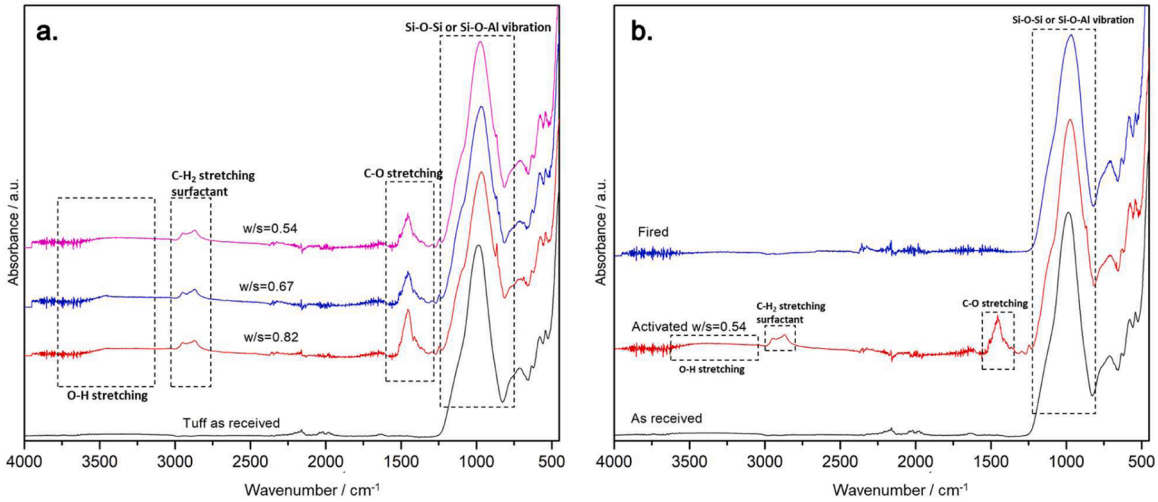

Fig. 10. FTIR diffraction patterns for (a) tuff foams obtained with different w/s ratio (b) tuff activated w/s = 0.54 in different conditions.

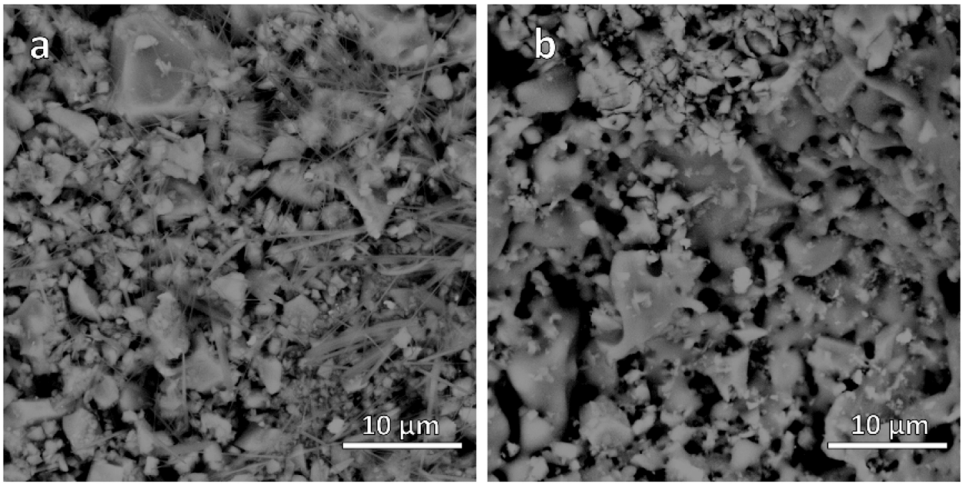

Fig. 11. Microstructural images of selected foam w/s = 0.54 (a) activated (b) fired.

Table 3
Physical and mechanical properties of foamed samples.

Sample type	Density [g/cm^3]	Total porosity (vol%)	Open porosity (vol%)	Closed porosity (vol%)	Compressive strength [MPa] [Bending strength of solid phase (MPa)]
Tuff foam_0.82	0.56 ± 0.01	77.8 ± 0.1	77.3 ± 0.1	0.5 ± 0.1	0.6 ± 0.1 [~26]
Tuff foam_0.67	0.75 ± 0.01	71.0 ± 0.1	69.5 ± 0.1	1.5 ± 0.1	1.4 ± 0.1 [~46]
Tuff foam_0.54	0.90 ± 0.01	64.7 ± 0.1	61.6 ± 0.1	3.1 ± 0.1	1.1 ± 0.1 [~26]
Tuff foam_0.82_fired	0.50 ± 0.01	81.7 ± 0.1	80.6 ± 0.1	1.1 ± 0.1	1.2 ± 0.2 [~76]
Tuff foam_0.67_fired	0.75 ± 0.01	72.5 ± 0.1	71.3 ± 0.1	1.2 ± 0.1	3.9 ± 0.1 [~135]
Tuff foam_0.54_fired	0.87 ± 0.02	68.6 ± 0.1	66.6 ± 0.1	2.0 ± 0.1	4.1 ± 0.2 [~117]

fired foams, in particular, overlap with refractory bricks.

A possible application concerns again lightweight concrete (all foams fall in the strength range of lightweight concrete, combined with a much lower density): beyond conventional processing, foams are suggested also for the development of skeletal mass made of compacted preplaced aggregates, later bound by forcing a flowable cement grout mixture through the voids, in the so-called two-stage concrete (TSC) [42,43]. It is worth to note that porous geopolymers derived from volcanic materials exhibit an excellent strength-to-density ratio (5.5–7 MPa cm^3/g [7–9]), well above that (~2 MPa cm^3/g) of the best present tuff-derived foams, in unfired state, but they are developed according to stronger activation and addition of valuable resources, such as aluminum powders [9]. Firing at 700 °C makes the strength-to-density of tuff-derived foams closer to that of porous geopolymers (5.2 MPa cm^3/g for '0.67_fired'

sample).

4. Conclusions

This study presents strategies for the exploitation of unemployed fraction of grey tuff in new sustainable construction materials, according to alkali activation. Despite being suspended in a low molarity activating solution, tuff powders (alone or added with waste glass) undergo consolidation, upon drying, by formation of strong bonds, resulting in bodies resisting to both boiling water and HCl solution (pH = 5). This result is promising in the perspective of a new generation of green binders, to be accompanied by a vast range of aggregates (object of future studies). A direct exploitation of this 'weak' activation approach, excluding further additives, is already feasible by application of heat treatment, at only 700 °C, and/or by foaming at the early stages of gelation, by intensive mechanical stirring. Porous bodies, in fact, fall in the strength range of lightweight concrete, with comparable or lower density.

Declaration of Competing Interest

We declare that we have no known competing financial, professional, or personal interests that could have appeared to influence the work reported in this paper.

Data Availability

Data will be made available on request.

Acknowledgements

The authors acknowledge the support of national project MUR PON R&I 2014–2021 (G.T.; H.E.; E.B.) and of "SusPIRe" (Sustainable porous ceramics from inorganic residues) project [BIRD202134, University of Padova, Dept. of Industrial Engineering)] (E.B.). The experimental assistance of Mr. Davide Beccarello (University of Padova) is also acknowledged.

Author agreement

This manuscript has not been published and is not under consideration for publication elsewhere. We have no conflicts of interest to disclose.

References

[1] J. Fikel, B.R. Bakshi, A. Baral, E. Guerra, B. Dequervain, Comparative life cycle assessment of beneficial applications for scrap tires, Clean. Technol. Environ. Policy 13 (2011), https://doi.org/10.1007/s10098-010-0289-1, 19-15.

[2] S.T. Blessen, Y. Jian, A. Bahurudeen, S.N. Chinnu, J.A. Abdalla, R.A. Hawileh, H. M. Hamada, Geopolymer concrete incorporating recycled aggregates: a comprehensive review, J. Clean. Prod. 3 (2022), 100056, https://doi.org/10.1016/j.clema.2022.100056.

[3] M. Amran, G. Murali, R. Fediuk, N. Vatin, Y. Vasilev, H. Abdelgader H, Palm oil fuel ash-based eco-efficient concrete: a critical review of the short-term properties, Materials 14 (2021) 332, https://doi.org/10.3390/ma14020332.

[4] J.L. Provis, Geopolymers and other alkali activated materials: why, how and what? Mater. Struct. 47 (2014) 11–25, https://doi.org/10.1617/s11527-013-0211-5.

[5] R.C. Kaze, G.L. Lecomte-Nana, E. Kamseu, P. Sanz Camacho, A.S. Yorkshire, J. L. Provis, M. Duttine, A. Wattiaux, U. Chinje Melo, Mechanical and physical properties of inorganic polymer cement made of iron-rich laterite and lateritic clay: a comparative study, Cem. Concr. Res. 140 (2021), 106320, https://doi.org/10.1016/j.cemconres.2020.106320.

[6] R.C. Kaze, A. Naghizadeh, L. Tchadjie, A. Adesina, J.N. Yankwa Djobo, J. Giogetti Deutou Nemaleu, E. Kamseu, U. Chinje Melo, B.A. Tayeh, Lateritic soils based geopolymer materials: a review, Constr. Build. Mater. 344 (2022), 128157, https://doi.org/10.1016/j.conbuildmat.2022.128157.

[7] L.M. Beleuk à Moungam, P.N. Lemougna, R.C. Kaze, H. Mohamed, J. Giogetti Deutou Nemaleu, N. Billong, E. Kamseu, A.D. Mvondo-Ze, I. Tonle Kenfack, Synthesis of volcanic ash-based porous inorganic polymers using biomass as pore inducing agent: phase evolution and descriptive microstructure, Silicon 14 (2022) 2595–2608, https://doi.org/10.1007/s12633-021-01004-8.

[8] L.M. Beleuk à Moungam, K.V. Tchieda, H. Mohamed, N. Chancellin Pecheu, R. C. Kaze, E. Kamseu, A.D. Mvondo-Ze, I. Tonle Kenfack, Efficiency of volcanic ash-based porous geopolymers for the removal of Pb^{2+}, Cd^{2+} and Hg^{2+} from aqueous solution, Clean. Mater. 5 (2022), 100106, https://doi.org/10.1016/j.clema.2022.100106.

[9] E. Kamseu, Z.N.M. NGouloure, B. Nait Ali, S. Zekeng, U.C. Melo, S. Rossignol, C. Leonelli, Cumulative pore volume, pore size distribution and phases percolation in porous inorganic polymer composites: relation microstructure and effective thermal conductivity, Energy Build. 88 (2015) 45–56, https://doi.org/10.1016/j.enbuild.2014.11.066.

[10] N. Toniolo, A.R. Boccaccini, Fly ash-based geopolymers containing added silicate waste. A review, Ceram. Int 43 (2017) 14545–14551, https://doi.org/10.1016/j.ceramint.2017.07.221.

[11] Q. Wan, R. Zhang, Y. Zhang, Structure and properties of phosphate-based geopolymer synthesized with the spent fluid catalytic-cracking (SFCC) catalyst, Gels 8 (2022) 130, https://doi.org/10.3390/gels8020130.

[12] L. Germinario, Á. Török, Variability of technical properties and durability in volcanic tuffs from the same quarry region - examples from Northern Hungary, Eng. Geol. 262 (2019), 105319, https://doi.org/10.1016/j.enggeo.2019.105319.

[13] N. Cobîrzan, G. Thalmaier, A.A. Balog, H. Constantinescu, A. Ceclan, M. Nasui, Volcanic tuff as secondary raw material in the production of clay bricks, Mater, Mater 14 (22) (2021) 2–14, https://doi.org/10.3390/ma14226872.

[14] A.T. Almalkawi, S. Hamadna, P. Soroushian, One-part alkali activated cement based volcanic pumice, Constr. Build. Mater. 157 (2017) 367–374, https://doi.org/10.1016/j.conbuildmat.2017.06.139.

[15] C. Pötzl, S. Siegesmund, R. López-Doncel, R. Dohrmann, Key parameters of volcanic tuffs used as building stone: a statistical approach, Environ. Earth Sci. 81 (2022) 10, https://doi.org/10.1007/s12665-021-10114-w.

[16] F. Pacheco-Torgal, J. Labrincha, C. Leonelli, A., Palombo, Handbook of alkali-activated cements, mortars and concretes, 2014.

[17] O. Öztürk, Engineering performance of reinforced lightweight geopolymer concrete beams produced by ambient curing, Struct. Concr. 23 (2022) 2076–2087.

[18] J.Ny Djobo, A. Elimbi, H.K. Tchakouté, S. Kuman, Volcanic ash-based geopolymer cements/concretes: the current state of the art and perspectives, JESPR 24 (5) (2017) 4433–4446.

[19] A.M. Zeyad, H.M. Magbool, B.A. Tayeh, A.R.G. de Azevedo, A. Abutaleb, Q. Hussain, Production of geopolymer concrete by utilizing volcanic pumice dust, Case Stud. Constr. Mater. 16 (2022), https://doi.org/10.1016/j.cscm.2021.e00802.

[20] K.E.H. Eldahroty, A.A. Farghali, N. Shehata, O.A. Mohamed, Valorification of Egyptian volcanic tuff as eco-sustainable blended cementitious materials, Sci. Rep. 13 (2023) 3653, https://doi.org/10.1038/s41598-023-30612-0.

[21] P. Guo, W. Meng, H. Nassif, H. Gou, Y. Bao, New perspectives on recycling waste glass in manufacturing concrete for sustainable civil infrastructure, Constr. Build. Mater. 257 (2020), 119579, https://doi.org/10.1016/j.conbuildmat.2020.119579.

[22] E. Bernardo, H. Elsayed, A. Mazzi, G. Tameni, S. Gazzo, L. Contrafatto, Double-life sustainable construction materials from alkali activation of volcanic ash/discarded glass mixture, Constr. Build. Mater. 359 (2022), 129540, https://doi.org/10.1016/j.conbuildmat.2022.129540.

[23] N. Toniolo, A. Rincon, J.A. Roether, P. Ercole, E. Bernardo, A.R. Boccaccini, Extensive reuse of soda-lime waste glass in fly ash-based geopolymers, Constr. Build. Mater. 188 (2018) 1077–1084, https://doi.org/10.1016/j.conbuildmat.2018.08.096.

[24] K. Felaous, A. Aziz, M. Achab, M. Fernández-Raga, A. Benzaouak, Optimizing alkaline activation of natural volcanic pozzolan for eco-friendly materials production: an investigation of NaOH molarity and Na_2SiO_3-to-NaOH ratio, Sustainability 15 (2023) 4453, https://doi.org/10.3390/su15054453.

[25] I.I. Bashar, U. Johnson Alengaram, M.Z. Jumaat, Enunciation of embryonic palm oil clinker based geopolymer concrete and its engineering properties, Constr. Build. Mater. 318 (2022), 125975, https://doi.org/10.1016/j.conbuildmat.2021.125975.

[26] A. Rincon Romero, G. Giacomello, M. Pasetto, E. Bernardo, Novel 'inorganic gel casting' process for the manufacturing of glass foams, J. Eur. Ceram. Soc. 37 (2017) 2227–2234, https://doi.org/10.1016/j.jeurceramsoc.2017.01.012.

[27] P.R. Monich, A.R. Romero, D. Höllen, E. Bernardo, Porous glass-ceramics from alkali activation and sinter-crystallization of mixtures of waste glass and residues from plasma processing of municipal solid waste, J. Clean. Prod. 188 (2018) 871–878, https://doi.org/10.1016/j.jclepro.2018.03.167.

[28] T. Kavas, Use of boron waste as a fluxing agent in production of red mud brick, Build. Environ. 41 (2006) 1779–1783, https://doi.org/10.1016/j.buildenv.2005.07.019.

[29] E.M. Pérez-Monserrat, L. Maritan, E. Garbin, G. Cultrone, Production technologies of ancient bricks from padua, italy: changing colors and resistance over time, Minerals 11 (7) (2021) 744, https://doi.org/10.3390/min11070744.

[30] S. Gudbrandsson, D. Wolff-Boenisch, Sigurdur R. Gislason, Eric H. Oelkers, Experimental determination of plagioclase dissolution rates as a function of its composition and pH at 22°C, Geochim. Consmochim. Acta 139 (2014) 154–172, https://doi.org/10.1016/j.gca.2014.04.028.

[31] M.A. Pereira, D.C.L. Vasconcelos, W.L. Vasconcelos, Synthetic aluminosilcates for geopolymer production, Mater. Res. 22 (2) (2019), https://doi.org/10.1590/1980-5373-MR-2018-0508.

[32] E. Ofer-Rozovsky, G. Bar-Nes, A. Katz, M.A. Haddad, Alkali activation of fly ash in the presence of sodium nitrate, Waste Biomass Valor 13 (2022) 2425–2446, https://doi.org/10.1007/s12649-021-01584-x.

[33] M. Catauro, F. Papale, G. Lamanna, F. Bollino, Geopolymer/PEG hybrid materials synthesis and investigation of the polymer influence on microstructure and

mechanical behavior, Mater. Res. 18 (4) (2015), https://doi.org/10.1590/1516-1439.342814.
[34] A.R. Romero, S. Tamburini, G. Taveri, J. Toušek, I. Dlouhy, E. Bernardo, Extension of the 'inorganic gel casting' process to the manufacturing of boro-alumino-silicate glass foams, Mater 11 (12) (2018) 2545, https://doi.org/10.3390/ma11122545.
[35] M. Ezzat, H.M. Khater, A.M. El Nagar, Enhanced characteristics of alkali activated slag/ grog geopolymer bricks, Int. J. Sci. Eng. 7 (2016) 230–243.
[36] M.C. Kennedy, E.D. Ford, P. Singleton, M. Finney, J.K. Agee, Informed multi-objective decision-making in environmental management using Pareto optimality, J. Appl. Ecol. 45 (2008) 181–192, https://doi.org/10.1111/j.1365-2664.2007.01367.x.
[37] E. Kaneva, R. Shendrik, Thermal behavior of natural stellerite: high-temperature X-ray powder diffraction and IR spectroscopy study, Anal. Sci. 38 (2022) 1523–1532, https://doi.org/10.1007/s44211-022-00186-4.
[38] N. Toniolo, G. Taveri, K. Hurle, J.A. Roether, P. Ercole, I. Dlouhy, A.R. Boccaccini, Fly-ash-based geopolymers: how the addition of recycled glass or red mud waste influences the structural and mechanical properties, J. Ceram. Sci. Technol. 08 (2017) 411–420, https://doi.org/10.4416/JCST2017-00053.
[39] X. Li, J. Zheng, J. Shao, M. Loutou, C. Bai, Y. Qiao, Y. Miao, X. Wang, T. Zheng, P. Colombo, Evaluation of porosity, mechanical and thermal properties of self-ignition coal gangue-based foams via fast microwave foaming, J. Build. Eng. 68 (2023), 106061, https://doi.org/10.1016/j.jobe.2023.106062.
[40] L.J. Gibson, M.F. Ashby, Cellular Solid, Structure and Properties, 2nd ed., Cambridge University Press, Cambridge, UK, 1999.
[41] E. Bernardo, G. Scarinci, A. Maddalena, S. Hreglich, Development and mechanical properties of metal–particulate glass matrix composites from recycled glasses, Compos. Part A: Appl. Sci. Manuf. 35–1 (2004) 17–22, https://doi.org/10.1016/j.compositesa.2003.09.022.
[42] H.S. Abdelgader, M. KurpiNska, M. Amran, Effect of slag coal ash and foamed glass on the mechanical properties of two-stage concrete, Mater. Today: Proc. 58 (2022) 1091–1097, https://doi.org/10.1016/j.matpr.2022.01.139.
[43] H.S. Abdelgader, A.S. El-Baden, H.A. Abdurrahman, A.S.M.Abdul Awal, Two-Stage Concrete as a Sustainable Production MATEC Web Conf. 149, 2018, 02009. ⟨https://doi.org/10.1051/matecconf/201814902009⟩.